Defect and Diffusion Forum
ISSN: 1662-9507, Vol. 426, pp 35-42
doi:10.4028/p-3d9axo

Submitted: 2022-09-06
Revised: 2022-12-05
Accepted: 2022-12-06
Online: 2023-06-06

P-Type Impurities in 4H-SiC Calculated Using Density Functional Theory

Niamh Smith[1,a*], Magdalena Weger[2,3,b], Gregor Pobegen[2,c], and Alexander Shluger[1,d]

[1]Department of Physics and Astronomy, University College London, Gower Street, London, WC1E 6BT, United Kingdom

[2]KAI GmbH, Europastrasse 8, 9524 Villach-St.Magdalen, Austria

[3]Johannes Kepler University Linz, Altenbergerstraße 69, 4040 Linz, Austria

[a]niamh.smith.17@ucl.ac.uk, [b] Magdalena.Weger2@k-ai.at, [c] gregor.pobegen@k-ai.at, [d]a.shluger@ucl.ac.uk

Keywords: P-Doping, Ion Implantation, Density Functional Theory (DFT)

Abstract. We have investigated the p-dopant potential of 14 different impurities (Be, B, F, Mg, Al, Ca, Sc, Cu, Zn, Ga, In, Ba, Pt, and Tl) within 4H-SiC via Density Functional Theory (DFT) calculations using a hybrid density functional. We analyse the incorporation energies of impurity atoms on Si and C sites as well as the character of lattice distortion induced by impurities. The calculated thermal ionization energies confirm that Al and Ga on the Si site are the best candidates for p-doping of 4H-SiC. Although we find some correlation of incorporation energies with atomic radii of impurities, the difference in chemical interaction with neighbouring atoms and strong lattice distortions play important roles in determining the impurity incorporation energies and charge transition levels. We find Al to still be the best and most industrially viable p-dopant for 4H-SiC.

Introduction

4H-SiC is a 3.26 eV band gap [1] semiconductor possessing a high critical breakdown field and thermal conductivity [2]. The properties of 4H-SiC allow it to be used within metal-oxide semiconductor field-effect transistor devices (MOSFETs) for high-power, high temperature electronics [3], such as telecoms, auxiliary inverters, and uninterruptible power supply appliances. For efficient usage, 4H-SiC's electrical conductivity must be enhanced via doping. This involves the addition of an impurity into 4H-SiC to generate free charge carriers as either electrons with energy levels close to that of the conduction band (E_C; n-type doping) or holes with energy levels close to that of the valance band (E_V; p-type doping).

P-type 4H-SiC is generally created via the implantation of Al^+ or B^+ ions in bulk 4H-SiC. B^+ ions can experience significant in- and out-diffusion when implanted in 4H-SiC, leading to elongation of junction depths and reductions in implanted atom concentrations, respectively [4]. Al^+ ions are preferentially used because lower acceptor levels [ionization energies] of hole states are achieved from implantation with aluminium [E_v+0.201 eV [5]], than from implantation with boron [E_V+0.300 eV [6]], once the implanted ions have been annealed into lattice sites. Almost 100% electrical activation of Al can be achieved during annealing of 4H-SiC at temperatures between 1600 and 1700 °C [4].

Several recently conducted experimental studies [7, 8, 9] have, however, discovered an association between a drop in device channel mobility, the formation of several unfavourable band gap states, and large Al implantation dosages. Id-DLTS measurements show that the density of one trap, with a similar activation energy to Al's ionization energy [E_v+0.135 to E_v+0.18 eV], is strongly positively correlated with the concentration of aluminium implanted into 4H-SiC during device creation [7], implying the formation of the trap band is directly related to the Al implantation dose used. A similar relationship was concluded from 2-dimensional density of states analysis between Al implantation dosage and the density of an interface state closer than 0.01 eV [8] to 4H-SiC's conduction band [9]. In all three studies, as trap band and interface state densities increased with increasing implantation dose,

device channel mobility decreased. Therefore, it appears the observed mobility drop is a direct consequence of the implantation of high Al concentrations into 4H-SiC, with aluminium being suggested to create carrier trapping defects [8] or even push 4H-SiC's Fermi level into the conduction band [9]. However, the identities of the aforementioned unfavourable band gap states and their doping-related formation mechanisms remain unknown. An alternative way forward would be to use other p-dopant species in the creation of p-type 4H-SiC MOSFET devices. However, no alternative dopants, which induce similar acceptor levels to Al, are currently known. We have investigated the p-doping potential of 4H-SiC, via calculating incorporation energy and acceptor levels of 12 possible alternative dopant impurities using hybrid density functional theory (DFT). In total, the potential of 14 different impurities have been explored, with Al and B also being investigated - in the same manner as the 12 possible alternative impurities - to deduce whether there is an alternative species to aluminium which can be used to p-dope 4H-SiC. The results presented here do not take into consideration any compensation or defect aggregation effects, such as impurity-vacancy complex formation, which may occur during ion implantation and anneal.

Methods

Computational details. All calculations were performed using the Gaussian Plane Wave (GPW) method [10], as implemented by the CP2K code [11], with the PBE0-TC-LRC hybrid density functional [12] and a cutoff energy of 600 Ry. An orthorhombic 7x4x1 supercell, containing 448 atoms, was adopted to simulate 4H-SiC at the Γ point. These hybrid DFT calculations are performed with 27% of Hartree-Fock (HF) exchange and predicts a 4H-SiC single electron band gap of 3.31eV, within 1.5% of experiment. All atomic species involved in simulations employed the consistent DZVP-MOLOPT-SR-GTH basis set [13], the DZP-UZH Auxiliary Density Matrix Methods basis set [14], and Goedecker, Teter and Hutter (GTH) pseudopotentials [15, 16, 17].

Modelling of impurity implantation. Before the inclusion of any impurities, we optimised 4H-SiC's structure inside of the 7x4x1 orthorhombic supercell. This resulted in primitive cell lattice constants of a = 3.09 Å and c = 10.06 Å, which are in good agreement with 4H-SiC's experimental room temperature lattice constants of a = 3.07 Å and c = 10.05 Å [7]. In this work we assume that the majority of the implanted dopant atoms substitute either Si or C in the lattice to form $X_{Si/C}$ defects (where X represents the impurity), rather than taking up interstitial positions within the 4H-SiC lattice. Each impurity atom was placed in a lattice site to replace a native Si/C atom and the geometry of the periodic cell was re-optimised. All calculations performed were spin polarised.

Screening impurities. The empirical approach of screening was taken to inform our choice of investigated impurities. Elements were evaluated for use as possible dopants based on two key screening characteristics: atomic valency and atomic radius. As Si and C are tetravalent elements, we have focused on impurities which are trivalent (to induce a hole in the β spin state) and divalent (to induce holes in both α and β spin states). We have studied four trivalent impurities - Ga, Sc, In, Tl - alongside Al and B, and 7 divalent impurities (Be, Mg, Ca, Cu, Zn, Ba, Pt). We have also investigated fluorine as a potential p-dopant due to a previous theoretical study, conducted with PBE, suggesting F may induce a shallower acceptor level than Al when placed interstitial [18]. In accordance with the site-competition theory [19], we have only created X_C defects with impurities that are of a similar atomic radius to carbon, i.e. X = Be, B, F, Mg, Al, and Ga. These impurities, except for Be, have also been investigated for X_{Si} defects alongside Ca, Sc, Cu, Zn, In, Pt, and Tl.

Impurity incorporation energy. Using 4H-SiC's experimentally determined heat of formation value (ΔH_f) of 0.72 eV [20], we have calculated each impurity's incorporation energy, $E_f[X_{Si/C}]$, at perfect stoichiometry ($\Delta\mu = 0$), and at the C-rich ($\Delta\mu = -\Delta H_f$) and Si-rich ($\Delta\mu = \Delta H_f$) limits via

$$E_f^0[X_{Si/C}] = E_{tot}[X_{Si/C}] - 0.5\left[(n_{Si} + n_C)\mu_{SiC_{bk}} + (n_{Si} - n_c)((\mu_{Si_{bk}} - \mu_{C_{bk}}) + \Delta\mu)\right] - n_X\mu_X \quad (1)$$

where $E_{tot}[X_{Si/C}]$ is the total energy of the supercell containing the $X_{Si/C}$ defect; n_{Si}, n_C, and n_X correspond to the number of Si, C, and impurity atoms within the defect containing supercell; and $\mu_{SiC_{bk}}$ is the total energy of defect-free 4H-SiC per formula unit [21]. We calculated $\mu_{SiC_{bk}}$ to be -262.4 eV. Chemical potentials $\mu_{Si_{bk}}$ and $\mu_{C_{bk}}$ are taken to be the total energies of silicon [$E(Si_{silicon})$ = -107.2 eV] and diamond [$E(C_{diamond})$ = -154.7 eV] per unit formula, respectively. Table 1 displays the corresponding chemical potentials μ_X of each impurity X.

Defining chemical potentials for different elements in a consistent manner is difficult. Not all of the investigated impurities form stable silicide or carbide compounds. Therefore, to maintain consistency when comparing different impurities, we have derived each impurity's chemical potential from the stable chloride compound they form with monovalent Cl, i.e. $\mu_X = E(XCl_n) - n\mu_{Cl}$, where n is the valency of the impurity and $\mu_{Cl} = \frac{1}{4}E(SiCl_4) - E(Si_{silicon})$ = -408.9 eV. These chlorides are non-metallic so enable the use of the PBE0 functional in all calculations.

Table 1: Used chemical potential for each of the explored impurities

X	Al	B	Ba	Be	Ca	Cu	F	Ga	In
μ_X	$AlCl_3$	BCl_3	$BaCl_2$	$BeCl_2$	$CaCl_2$	$CuCl_2$	ClF_3	$GaCl_3$	$InCl_3$
eV	-58.1	-76.3	-698.1	-400.5	-1004.2	-1296.5	-656.5	-2014.7	-1521.7

X	Mg	Sc	Pt	Tl	Zn
μ_X	$MgCl_2$	$ScCl_3$	$PtCl_2$	$TlCl_3$	$ZnCl_2$
eV	-1722.5	-1273.7	-3267.0	-1347.1	-1634.1

Impurity acceptor level. To compare defect levels induced by different dopants, we calculated both thermal ionization energies and single electron Kohn-Sham (e^- KS) defect levels. Thermal ionization energy (TIE) is taken to be the Fermi energy above the defect-free structure's valence band maximum (VBM) at which the formation energies of a defect structure in the neutral and the first negatively charged states intersect, commonly termed the 0/-1 charge transition level [22, 23]. It is calculated as a difference in total system energies, as described in eq. (1), with an additional correction term due to the interaction of periodic images of charged defects:

$$E_f^q[X_{Si/C}] = E_f^0[X_{Si/C}] + q(\varepsilon_{VBM} + \delta\varepsilon_f) + E_{corr}, \quad (2)$$

where q is the charge of the supercell, ε_{VBM} is the energy level of the defect-free structure's VBM, and $\delta\varepsilon_f$ is the Fermi energy [24]. To calculate the charge correction term E_{corr}, we have used the anisotropic Makov-Payne point charge correction [25, 26]. TIE is the thermal energy required to create a hole in the valence band via populating the unoccupied dopant state in the SiC band gap. Single e^- KS level refers to the difference between the highest occupied molecular orbital (HOMO) and the lowest unoccupied molecular orbital (LUMO) KS eigenvalues of a particular spin state [27]. In a defect free structure, both spin state KS levels will be equal to the predicted band gap of the material. However, in a structure containing 1 or 2 hole states, the LUMO state of either one or both spin states will be in the band gap. The electronic structures of each substitutional defect-related HOMO and LUMO KS molecular orbitals have also been examined. In particular, some of the defects strongly perturb the SiC lattice and electronic structure and induce so-called quasi-local states in the valence band. For each defect We report energy difference between the last completely delocalised molecular orbital at the top of the VB and its first unoccupied molecular orbital in the gap. This is because a hole is unable to act as an effective charge carrier if its density is partially localised in a quasi-local state.

Results and Discussion

We start from discussing the results obtained for impurity incorporation energies into Si and C sites. These depend on the chemical potential used in calculations. Consequently, directly comparing absolute incorporation energy values between all impurities may be misleading, as the ionic nature of the

chloride compounds used to derive impurity chemical potentials vary quite considerably. We discuss relative values for subsets of impurities: Zn, Cu, and Pt [μ derived from chlorides of declining ionic nature]; Mg, Ca, Ba [μ derived from homogeneous ionic chlorides]; and Al, Ga, In, Tl [μ derived from ionic chlorides]. In this short report we only consider substitution of Si and C sites and omit results for interstitial single impurity positions.

Fig. 1 displays our calculated incorporation energies for all impurity substitutional defect sites evaluated under Si-rich, stoichiometric, and C-rich environments. Under C-rich conditions, the excess of carbon generates surface degradation of 4H-SiC effecting the carbon coverage of grown surfaces. Si-rich conditions, on the other hand, can alter the morphology of 4H-SiC's surface due to the formation of Si-droplets. Experimental investigations have shown that alteration of surface coverage of Si and C, through different growth environmental conditions, directly impacts the incorporated concentration of a dopant [28].

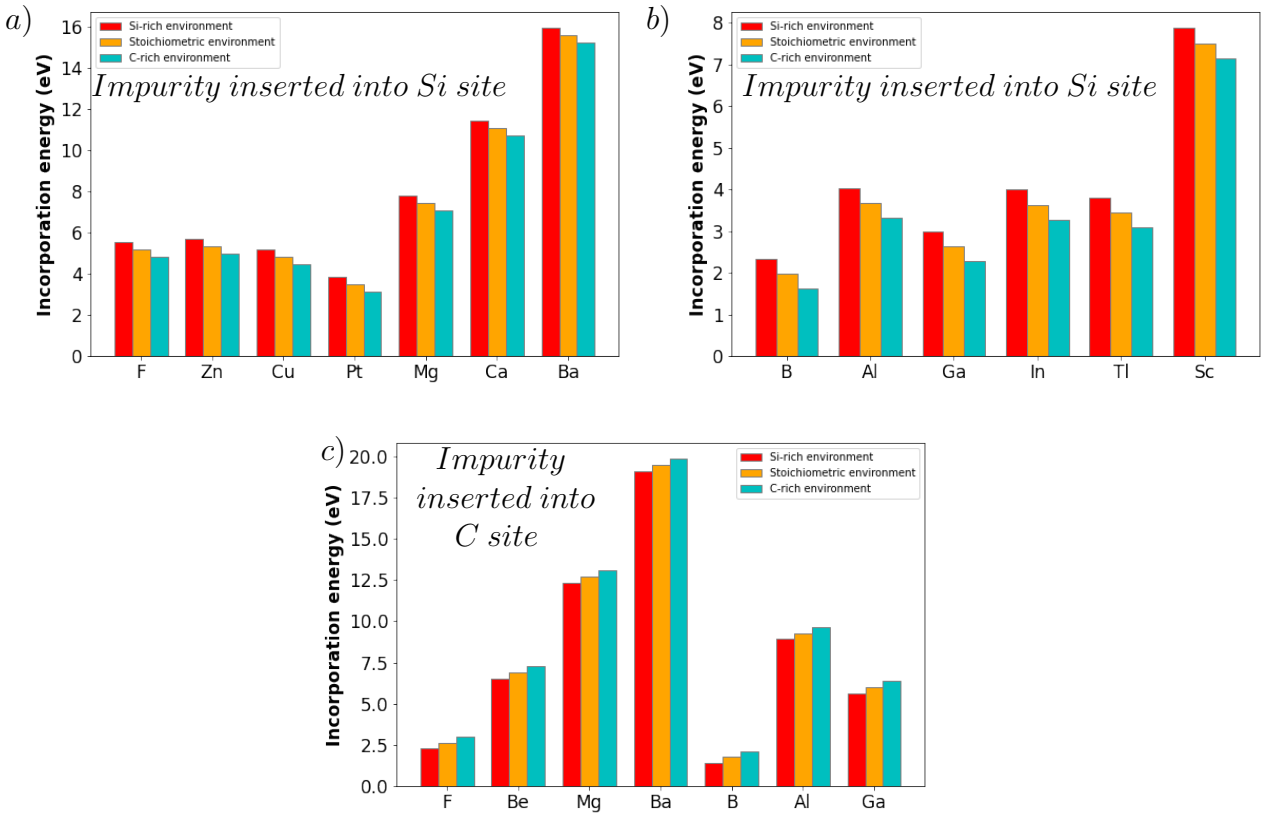

Fig. 1: Incorporation energy derived for $a)$ the X_{Si} defect when X is equal to F and divalent impurities Zn, Mg, Cu, Ca, Pt, and Ba; $b)$ the X_{Si} defect when X is equal to trivalent impurities B, Al, Ga, In, Tl, and Sc; $c)$ the X_C defect when X is equal to F, Be, Mg, Ba, B, Al, and Ga. For each impurity incorporation energies have been calculated under Si-rich (red, left bar), C-rich (blue, right bar), and stoichiometric (orange, middle bar) environmental conditions.

As can be seen, impurity incorporation on the X_{Si} defect site requires the most energy when under Si-rich conditions and the least when under C-rich conditions; while the opposite is true for impurity incorporation on the X_C defect site. The x-axis ordering of impurities on each graph within Fig. 1 is in accordance with increasing valency and atomic radius [29], from left to right, amongst investigated impurities on each substitutional site. For the Si site, monovalent and divalent impurity incorporation energies can be seen in Fig 1a, while trivalent impurities are presented in Fig 1b. Empirical atomic radii values can be found in tables 2 and 3 alongside maximum nearest neighbour displacement values,

single e^- KS levels, and ionization energies for impurities substituted in the X_{Si} and X_C defect sites, respectively.

Table 2: Investigated possible dopant impurities for the Si-substitutional site, X_{Si}. Δx_{max} is the maximum displacement [Å] of neighbouring C atoms around the X_{Si} defect, Δx_{Si-X} is the displacement [Å] of the impurity's atom from the centre of the host Si atom it has replaced, $E_f^0[X_{Si}]_{stoi}$ is the Stoichiometric incorporation energy [eV] of the defect, and IE is the defect's ionization energy [eV]. references: [a] [29], [b] [30], [c] [6], [d] [5], [e] [31], [f] [32].

Dopant impurity (X)	Valency	Atomic radii [Å][a]	Computational results for defect						Exp. acceptor level [eV]
			Δx_{max}	Δx_{Si-X}	$E_f^0[X_{Si}]_{stoi}$	Single e^- KS level [eV] α spin	Single e^- KS level [eV] β spin	IE	
F	1	0.57	0.30	0.65	5.18	2.80	2.57	3.42	-
Zn	2	1.22	0.22	0.11	5.34	0.98	0.91	0.65	-
Cu	2	1.32	0.14	0.03	4.81	1.28	1.40	1.41	-
Pt	2	1.36	0.20	0.04	3.51	1.09	1.09	1.75	-
Mg	2	1.41	0.63	0.33	7.46	0.98	0.98	0.69	>0.5[b]
Ca	2	1.76	0.45	0.17	11.06	1.47	1.47	1.31	-
Ba	2	2.15	0.62	0.24	15.57	1.56	1.56	1.97	-
B	3	0.84	0.17	0.32	1.98	3.30	1.51	0.37	0.3,0.65[c]
Al	3	1.21	0.14	0.01	3.67	3.32	0.18	0.18	0.20[d]
Ga	3	1.22	0.18	0.02	2.63	3.32	0.34	0.27	0.27[e]
In	3	1.42	0.30	0.01	3.63	3.30	0.48	0.38	-
Tl	3	1.45	0.30	0.07	3.44	3.28	0.64	0.52	-
Sc	3	1.70	0.37	0.08	7.51	3.29	1.10	0.55	0.55[f]

Incorporation energies are determined by the amount of perturbation created within a crystal structure upon insertion of an impurity. Incorporation of foreign atoms creates structural distortions in two main ways corresponding to the positioning of the impurity in the host site and the character of relaxation experienced by atoms surrounding the impurity. Therefore, we must consider atomic radii and nearest neighbour displacements alongside incorporation energy. Most of the impurities considered here have larger atomic radii than host atoms, which contributes to their large incorporation energies. The character of lattice distortion induced by impurities is illustrated in Figure 2 for two characteristic examples of In and Ca atoms on the Si site. We note that In is trivalent and Ca is divalent with s character of valence electrons. Therefore the bond hybridisation characteristic for SiC is strongly disrupted in both cases. Both ions are displaced from the host crystallographic site and induce large asymmetric displacements of surrounding carbon atoms. The character of chemical bonding and lattice distortions induced by other impurities will be discussed in detail in separate publication.

Thermal ionization energies characterize the utility of dopants. We note that all trivalent impurities were calculated to have TIEs below 0.6eV. Compared to experimental acceptor values, our results are in very good agreement, with only slight variations of 0.02 and 0.07eV for Al and B (we have taken the first acceptor level of 0.3 eV [6] to be equivalent to the B_{Si} defect), respectively. Investigation of the electronic structures of β spin HOMO KS eigenvalues for Al_{Si}, Ga_{Si}, and In_{Si} showed quasi-localisation of electron density, with density partially localised around each defect site. For each other these defects, the HOMO-1 molecular orbital was found to be the highest delocalised orbital. Due to this, KS levels have been corrected to extend from the HOMO-1 to the LUMO KS molecular orbitals for these defects. Zn and Mg are also the only two divalent impurities which have TIEs under 1 eV.

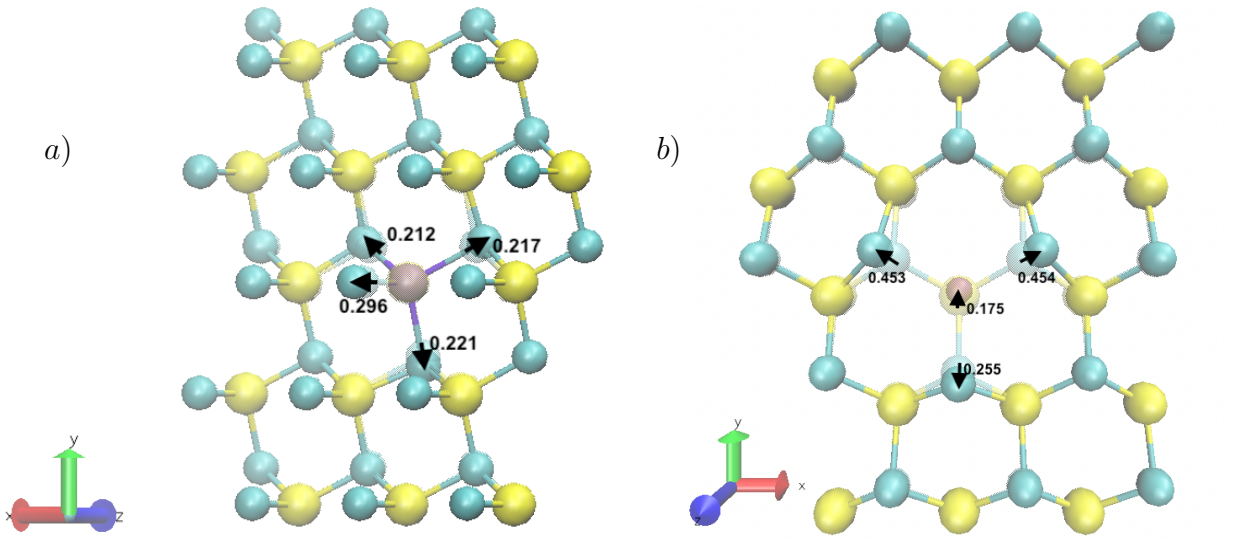

Fig. 2: Local lattice distortions induced by impurities on Si site in 4H-SiC. Arrows show the directions of displacements of C atoms nearest to impurity and numbers are values of distortions in Å. a) In atom substituting Si, and b) Ca atom substituting Si. Note different projections used.

Fluorine is predicted to have TIE larger than the 4H-SiC's bandgap, so cannot be used as a dopant at all when placed in the X_{Si} site

By analysing tables 2 and 3 one can deduce that, in general, KS levels are inaccurate and do not align with TIE counterparts for the X_{Si} defect site, even when quasi-localisation of the HOMO molecular orbital has been accounted for. The most dramatic case of this can be seen in the β spin KS level of B_{Si}. Al and Cu are the only two impurities which have roughly equal β spin KS levels to their ionization energy. Surprisingly, moreover, Cu and Al induce the same maximum displacements of surrounding atoms of 0.14 Å . Out of all impurities assessed in the X_{Si} site, 0.14 Å is the smallest maximum displacement seen. From this, it could be suggested that KS levels can be used as relatively accurate indicators when perturbation caused by impurity insertion is minimal.

Different behaviour overall in incorporation energy is seen amongst the impurities inserted into the carbon site. Incorporation energy is seen clearly to increase as a function of difference in atomic radii between C (radius 0.69 Å [29]) and impurity atom. The only exception is Ga. Despite having an atomic radius 0.53 Å larger than C, Ga's incorporation energy is predicted to fall in between the incorporation energies of F and Be, which have atomic radii difference of 0.12 and 0.27 Å compared to C, respectively.

Boron is found to have the lowest ionization energy on the X_C site and displaces its neighbouring carbons the least. This is consistent with the notion that atomic substitution is most favourable when minimal structural perturbation occurs. The calculated ionization energy of B on the X_C site agrees very well (within 0.02 eV) with the second experimentally determined acceptor level of boron [6]. Comparing the results for boron occupation of both X_{Si} and X_C defect sites, it can be seen that it is more energetically favourable, by 0.22 eV, for boron to occupy the X_C site but the acceptor level of this site is double the acceptor level of B_{Si}. This is in agreement with previous work [6] which identifies the shallow and deep acceptor levels of B in 4H-SiC.

As for the other impurities assessed in both the X_{Si} and X_C sites, apart from F, all have larger incorporation energies and TIEs when in the X_C site compared to the X_{Si} site. The F_C defect's incorporation energy is just slightly over half of F's incorporation energy in the X_{Si} site and has a deep ionization level in 4H-SiC's band gap.

To summarise, our results confirm that Al and Ga on Si site are the best candidates for p-doping of 4H-SiC. Although we find some correlation of incorporation energies with atomic radii of impuri-

Table 3: Investigated possible dopant impurities for the C-substitutional site, X_C. Δx_{max} is the maximum displacement [Å] of neighbouring Si atoms around the X_C defect, Δx_{C-X} is the displacement [Å] of the impurity's atom from the centre of the host C atom it has replaced, $E_f^0[X_C]_{stoi}$ is the Stoichiometric incorporation energy [eV] of the defect, and IE is the defect's ionization energy [eV]. references: [a] [29], [b] [33], [c] [6], [d] [5], [e] [31].

Dopant impurity (X)	Valency	Atomic radii [Å][a]	Computational results for defect						Exp. acceptor level [eV]
			Δx_{max}	Δx_{C-X}	$E_f^0[X_C]_{stoi}$	Single e^- KS level [eV] α spin	β spin	IE	
F	1	0.57	0.47	0.81	2.65	1.11	2.65	2.88	-
Be	2	0.96	0.19	0.02	6.89	1.29	1.32	1.57	0.59,1.0[b]
Mg	2	1.41	1.04	0.71	12.71	1.10	1.10	2.14	-
Ba	2	2.15	0.94	0.08	19.47	0.71	0.84	2.43	-
B	3	0.84	0.07	0.10	1.76	3.26	0.84	0.63	0.3,0.65[c]
Al	3	1.21	0.34	0.05	9.29	2.34	1.00	1.79	0.20[d]
Ga	3	1.22	0.32	0.08	6.00	2.57	0.97	1.55	0.27[e]

ties, the difference in chemical interaction with neighbouring atoms and strong lattice distortions play important roles in determining the impurity incorporation energies and charge transition levels. We note that further studies taking into consideration compensation or defect aggregation effects, such as impurity-vacancy complex formation, which may occur during ion implantation and anneal, are required to reach more definite conclusions.

Acknowledgments

NS would like to thank EPSRC and Infineon Technologies, Austria for financial support. Via our membership of the UK's HEC Materials Chemistry Consortium, which is funded by EPSRC (EP/R029431), this work has been completed using the ARCHER2 UK National Supercomputing Service (http://www.archer2.ac.uk). The authors are grateful to M. Bockstedte for valuable discussions.

References

[1] W.J. Choyke and G. Pensl: *Mrs Bulletin* Vol. 22, no. 3 (1997), pp. 25-29.

[2] M. Miyata and Y. Hayafuji: *Applied physics express* Vol. 1, no. 11 (2008), p. 111401.

[3] F. Roccaforte, P. Fiorenza, M. Vivona, G. Greco and F. Giannazzo: *Materials* Vol. 14, no. 14 (2021), p. 3923.

[4] T. Kimoto and J.A. Cooper: *Fundamentals of silicon carbide technology: growth, characterization, devices and applications*, John Wiley and Sons (2014).

[5] I.G. Ivanov, A. Henry and E. Janzén: *Physical Review B* Vol. 71, no. 24 (2005), p. 241201.

[6] S.G. Sridhara, L.L. Clemen, R.P. Devaty, W.J. Choyke, D.J. Larkin, H.S. Kong, T. Troffer and G. Pensl: Journal of applied physics Vol. 83, no. 12 (1998), pp. 7909-7919.

[7] J.V. Berens: PhD diss., Wien, (2021).

[8] T. Kobayashi, S. Nakazawa, T. Okuda, J. Suda and T. Kimoto: *Applied Physics Letters* Vol. 108, no. 15 (2016), p. 152108.

[9] T. Kobayashi, S. Nakazawa, T. Okuda, J. Suda and T. Kimoto: *Journal of Applied Physics* Vol. 121, no. 14 (2017), p. 145703.

[10] F. Aryasetiawan and O. Gunnarsson: *Reports on Progress in Physics* Vol. 61, no. 3 (1998), p. 237.

[11] T.D. Kühne, M. Iannuzzi, M. Del Ben, V.V. Rybkin, P. Seewald, F. Stein, T. Laino, et al: *The Journal of Chemical Physics* Vol. 152, no. 19 (2020), p. 194103.

[12] C. Adamo and V. Barone: *The Journal of chemical physics* Vol. 110, no. 13 (1999), pp. 6158-6170.

[13] J. VandeVondele and J. Hutter: *The Journal of chemical physics* Vol. 127, no. 11 (2007), p. 114105.

[14] M. Guidon, J. Hutter and J. VandeVondele: *Journal of chemical theory and computation* Vol. 6, no. 8 (2010), pp. 2348-2364.

[15] S. Goedecker, M. Teter and J. Hutter: *Physical Review B* Vol. 54, no. 3 (1996), p. 1703.

[16] C. Hartwigsen, S. Gœdecker and J. Hutter: *Physical Review B* Vol. 58, no. 7 (1998), p. 3641.

[17] M. Krack: Theoretical Chemistry Accounts Vol. 114, no. 1 (2005), pp. 145-152.

[18] M. Miyata, S. Hattori and Y. Hayafuji: *Japanese Journal of Applied Physics* Vol. 48, no. 4R (2009), p. 041301.

[19] D.J. Larkin in: *Inst. Phys. Conf. Ser* no. 142 (1995)

[20] S. Fahy, X.W. Wang and S.G. Louie: *Physical Review B* Vol. 42, no. 6 (1990), p. 3503.

[21] J.E. Northrup and S.B. Zhang: *Physical Review B* Vol. 47, no. 11 (1993), p. 6791.

[22] S.B. Zhang and J.E. Northrup: Physical review letters Vol. 67, no. 17 (1991), p. 2339.

[23] C. Freysoldt, B. Grabowski, T. Hickel, J. Neugebauer, G. Kresse, A. Janotti and C.G. Van de Walle: Reviews of modern physics Vol. 86, no. 1 (2014), p. 253.

[24] H.P. Komsa, T.T. Rantala and A. Pasquarello: Physical Review B Vol. 86, no. 4 (2012), p. 045112.

[25] G. Makov and M.C. Payne: Physical Review B Vol. 51, no. 7 (1995). p. 4014.

[26] S.T. Murphy and N.D. Hine: Physical Review B Vol. 87, no. 9 (2013), p. 094111.

[27] R. Stowasser and R. Hoffmann: Journal of the american chemical society Vol. 121, no. 14 (1999), pp. 3414-3420.

[28] I.R. Arvinte: PhD diss., COMUE Université Côte d'Azur (2016).

[29] B. Cordero, V. Gómez, A.E. Platero-Prats, M. Revés, J. Echeverría, E. Cremades, F. Barragán and S. Alvarez: Dalton Transactions Vol. 21 (2008), pp. 2832-2838.

[30] H. Matsuura, T. Morine and S. Nagamachi: Jpn. J. Appl. Phys. Vol. 54 (2015), p. 011301

[31] T. Kimoto, A. Yamashita, A. Itoh and H. Matsunami: Japanese journal of applied physics Vol. 32, no. 3R (1993), p. 1045.

[32] C. Haberstroh, , R. Helbig, and R. A. Stein: Journal of applied physics Vol. 76, no. 1 (1994), pp. 509-513.

[33] M. Krieger, M. Laube, M. Weidner and G. Pensel: Beryllium-Related Defect Centers in 4H-SiC (Trans Tech Publications, Switzerland 2001).